CANCER BIOTHERAPY AND RADIOPHARMACEUTICALS
Volume 33, Number 9, 2018
Mary Ann Liebert, Inc.
DOI: 10.1089/cbr.2018.2505

Biodistribution and Internal Radiation Dosimetry of ^{99m}Tc-IDA-D-[c(RGDfK)]$_2$ (BIK-505), a Novel SPECT Radiotracer for the Imaging of Integrin $\alpha_v\beta_3$ Expression

Yoo Sung Song,[1,*] Joong Hyun Kim,[2,*] Byung Chul Lee,[1,3] Jae Ho Jung,[1] Hyun Soo Park,[1,4] and Sang Eun Kim[1,3,4]

Abstract

Background: Integrin $\alpha_v\beta_3$ is a molecular marker for the estimation of tumor angiogenesis. ^{99m}Tc-IDA-D-[c(RGDfK)]$_2$ (also known as BIK-505) is a recently developed radiotracer for single-photon emission computed tomography, with good affinity for integrin $\alpha_v\beta_3$. In this study, the authors investigated the whole-body distribution and internal radiation dosimetry of ^{99m}Tc-IDA-D-[c(RGDfK)]$_2$ in elderly human participants.

Materials and Methods: Six healthy volunteers underwent whole-body simultaneous anterior and posterior scans, preceded by transmission scans using cobalt-57 flood source, with a dual head gamma camera system, at 0, 1, 2, 4, 8, and 24 h postinjection of ^{99m}Tc-IDA-D-[c(RGDfK)]$_2$ (injected radioactivity [mean ± SD] = 388.7 ± 29.3 MBq). Anterior and posterior images were geometrically averaged and attenuation corrected to delineate the regions of interest in the liver, gallbladder, kidneys, urinary bladder, spleen, brain, and large intestine. Radiation dose for each organ and the effective doses (EDs) were estimated using OLINDA/EXM 1.1 software.

Results: High radiation doses of renal and biliary excretion tracks such as the urinary bladder wall, upper large intestine, kidneys, liver, and gallbladder wall (19.15 ± 6.84, 19.28 ± 4.78, 15.67 ± 0.90, 9.13 ± 1.71, and 9.09 ± 2.03 μGy/MBq, respectively) were observed. The ED and effective dose equivalent were 5.08 ± 0.53 and 7.11 ± 0.58 μSv/MBq, respectively.

Conclusions: Dosimetry results were comparable to other radiolabeled peptides and were considered safe and efficient for clinical usage.

Keywords: ^{99m}Tc-IDA-D-[c(RGDfK)]$_2$, angiogenesis, biodistribution, dosimetry, integrin $\alpha_v\beta_3$ expression

Introduction

Angiogenesis is the process of new blood vessel formation from the preexisting vasculature. It is well accepted as a biomarker for the growth, invasion, and metastasis of numerous solid tumors.[1–3] Currently, there is a growing demand for novel noninvasive *in vivo* imaging techniques for response assessment and the pretherapeutic stratification of patients receiving antiangiogenic therapies. It has been suggested that angiogenesis-targeted imaging can provide an early diagnosis and aid in treatment planning and the monitoring of antiangiogenic cancer therapies.[4–6]

[1]Department of Nuclear Medicine, Seoul National University Bundang Hospital, Seoul National University College of Medicine, Seongnam, Republic of Korea.
[2]Division of Chemical and Medical Metrology, Center for Ionizing Radiation, Korea Research Institute of Standards and Science, Daejeon, Republic of Korea.
[3]Center for Nanomolecular Imaging and Innovative Drug Development, Advanced Institutes of Convergence Technology, Suwon, Republic of Korea.
[4]Department of Transdisciplinary Studies, Graduate School of Convergence Science and Technology, Seoul National University, Seoul, Republic of Korea.
*These authors contributed equally to this work.

Address correspondence to: Sang Eun Kim; Department of Nuclear Medicine, Seoul National University Bundang Hospital; 82, Gumi-ro 173 Beon-gil, Bundang-gu, Seongnam 13620, Republic of Korea **or** ***Hyun Soo Park; Department of Transdisciplinary Studies, Graduate School of Convergence Science and Technology, Seoul National University; Suwon 16229, Republic of Korea***
E-mail: **kse@snu.ac.kr** ***or*** **hyuns@snu.ac.kr**

Integrin $\alpha_v\beta_3$ is a suitable target for both tumor angiogenesis imaging and antiangiogenic therapy because of its high expression on activated endothelial cells and new blood vessels found in tumors and surrounding tissues, while it is absent in most intact normal tissues.[7,8] Therefore, integrin $\alpha_v\beta_3$ is considered an indicator of activated angiogenesis; imaging of integrin $\alpha_v\beta_3$ overexpression is a promising technique for the assessment of angiogenesis. Labeled synthetic ligands with demonstrated specificity for integrin $\alpha_v\beta_3$ have proven to be successful agents for *in vivo* imaging of tumor angiogenesis.[4] In particular, agents based on the amino acid sequence Arg-Gly-Asp (RGD) have been identified as useful for tumor angiogenesis imaging.[9–11] A significant correlation between the tracer uptake and the level of angiogenesis has been demonstrated in clinical *in vivo* studies of tumor imaging performed using radiolabeled RGD peptides.[12,13]

IDA-D-[c(RGDfK)]$_2$ is a newly developed, cyclic synthetic ligand containing the RGD binding site, with a high affinity ($IC_{50} = 50$ nM) for integrin $\alpha_v\beta_3$ during angiogenesis.[14] Preclinical imaging studies using ^{99m}Tc-IDA-D-[c(RGDfK)]$_2$ (also known as BIK-505) and single-photon emission computed tomography (SPECT) have demonstrated substantial and specific uptake of the radiotracer at the sites of integrin $\alpha_v\beta_3$ overexpression in tumors[14] and high-risk atherosclerotic plaques in discrimination with inflammation.[15] Moreover, a recently published human study demonstrated the preliminary clinical efficacy of ^{99m}Tc-IDA-D-[c(RGDfK)]$_2$ SPECT in the visualization and localization of activated angiogenesis in brain and lung tumors.[16] In the study, angiogenesis imaging using ^{99m}Tc-IDA-D-[c(RGDfK)]$_2$ SPECT facilitated the visualization of integrin $\alpha_v\beta_3$ overexpression in both lung and brain tumors, with no laboratory and clinical adverse events, whereas the relationship between the level of active angiogenesis and glucose metabolism (measured with 2-[^{18}F]fluoro-2-deoxyglucose and positron emission tomography) was different between lung and brain tumors. Thus, ^{99m}Tc-IDA-D-[c(RGDfK)]$_2$ SPECT is a potential tool for the *in vivo* assessment of angiogenesis through the visualization of integrin $\alpha_v\beta_3$ overexpression in solid tumors.

Human internal radiation dosimetry for a newly developed radiotracer is essential for the risk-benefit assessment of clinical application. In this study, the authors evaluated the whole-body distribution and radiation dosimetry of ^{99m}Tc-IDA-D-[c(RGDfK)]$_2$ in healthy volunteers using serial emission data sets obtained using a dual head gamma camera system.

Materials and Methods

Healthy volunteers

The present study was approved by the Institutional Review Board of the Seoul National University Bundang Hospital (IRB No.: B-1112-069-004). Informed consent was obtained from all of the individual participants. All the procedures performed were in accordance with the ethical standards of the institutional research committee and with the 1964 Helsinki Declaration and its later amendments or comparable ethical standards.

The participants were recruited through Internet advertisements and a hospital bulletin board. Six healthy participants (male:female = 2:4; mean age ± SD = 68.3 ± 3.2 years [range, 64–73 years]; mean body weight ± SD = 56.5 ± 10.7 kg [range, 47–77 kg]) voluntarily participated in the study. Participants were age matched with their previous study against brain tumor and lung cancer patients.[16] They had no clinically significant medical or neurologic conditions and presented with no clinically significant abnormalities on physical, neurologic, and laboratory examinations.

Preparation of ^{99m}Tc-IDA-D-[c(RGDfK)]$_2$

The precursor IDA-D-[c(RGDfK)]$_2$ was generously provided by Bio Imaging Korea Co. Ltd. (Seoul, Republic of Korea), which owns the intellectual property rights. Sodium pertechnetate (^{99m}Tc) was eluted daily from ^{99}Mo/^{99m}Tc-generator (Samyoung Unitech, Seoul, Republic of Korea). Structure of ^{99m}Tc-IDA-D-[c(RGDfK)]$_2$ is provided in Figure 1. ^{99m}Tc-IDA-D-[c(RGDfK)]$_2$ was synthesized following the method described in their previous work.[14] A solution of $[^{99m}Tc(H_2O)_3(CO)_3]^+$ (370-740 MBq) in saline (200 μL) prepared according to the protocol described by Alberto et al.[17] was added to the precursor in water (300 μL). After stirring the reaction mixture at 75°C for 30 min, the obtained ^{99m}Tc-IDA-D-[c(RGDfK)]$_2$ was purified using semipreparative high-performance liquid chromatography (HPLC; Eclipse XDB-C18 column; 5 mm, 9.4 × 250 mm; Agilent Co., Palo Alto, CA). Their current study followed the same gradient conditions. All radiochemical processes, including ^{99m}Tc incorporation, HPLC purification, and tC_{18} Sep-Pak cartridge purification, were conducted within 60 ± 5 min. A quality control check, including pH, endotoxin testing, analytic HPLC, and residual solvents measurement by gas chromatography, was performed before human use; a radiochemical purity of 95% was mandatory. Molar radioactivity of ^{99m}Tc-IDA-D-[c(RGDfK)]$_2$; 3.8 Ci/μmol (the injected chemical dose = 63 ng/kg) was obtained after HPLC purification.

Data acquisition

Participants were asked to urinate before the injection of ^{99m}Tc-IDA-D-[c(RGDfK)]$_2$. Philips ADAC Forte dual-head gamma camera (Philips Medical Systems, Andover, MA) was used to acquire transmission and serial emission scan data sets. The photopeak was centered at 140 keV in a 20% width energy window using low-energy high-resolution collimators. Whole-body transmission scan was performed for attenuation correction using a Cobalt-57 flood source just before the injection of ^{99m}Tc-IDA-D-[c(RGDfK)]$_2$. After the transmission scan, acquisition of simultaneous anterior and posterior whole-body emission scans was started at 0, 1, 2, 4, 8, and 24 h postinjection of 388.7 ± 29.3 MBq of ^{99m}Tc-IDA-D-[c(RGDfK)]$_2$. The dose administrated was based on data from previous ^{99m}Tc-labeled RGD image studies.[16,18–20] The scan speed was 20 cm/min for the whole body for both the transmission and emission scans. The duration of each whole-body scan was about 10.7 min.

The posterior image was mirrored, and the anterior-to-posterior pixel-by-pixel geometric average of the counts was determined. The calibration factor [(counts/pixel)/(Bq/pixel)] was obtained to convert counts/pixel into Bq/pixel using whole-body counts and injected doses (MBq). The attenuation was corrected using the transmission scan data and geometrically averaged first emission scan data under an assumption that the subject did not move during the transmission and first emission scans. Attenuation correction factors of the organs were obtained from attenuation corrected and nonattenuation corrected first scan data and were applied to all time-activity curves of the regions of interest (ROIs).

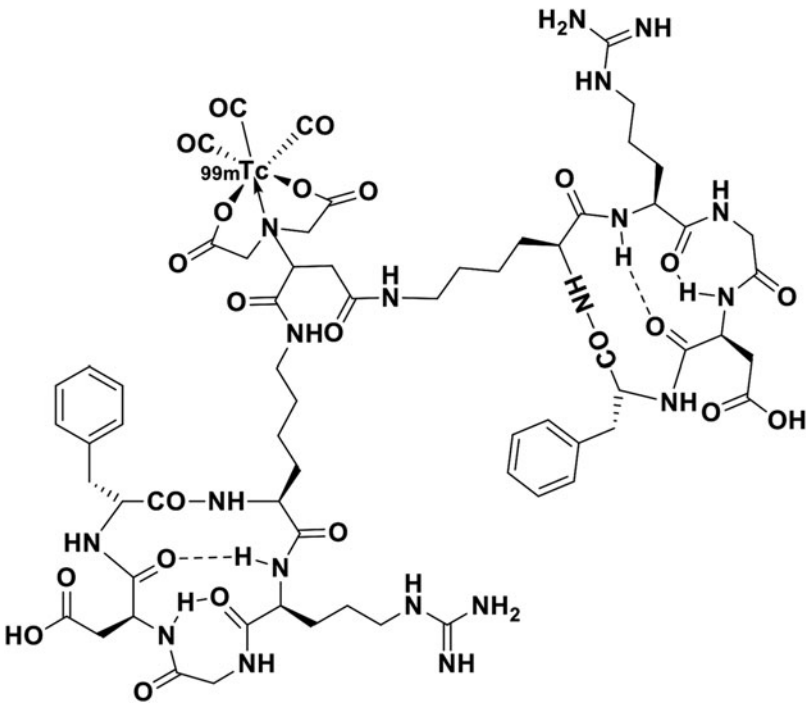

FIG. 1. Chemical structure of ^{99m}Tc-IDA-D-[c(RGDfK)]$_2$.

Quantitative analysis and radiation dose estimation

ROIs were manually drawn over the whole-body images at each time point, identifying high uptake organs such as the liver, kidneys, urinary bladder, gallbladder, spleen, brain, and large intestine to obtain the time-activity curves. The radioactivity of ^{99m}Tc-IDA-D-[c(RGDfK)]$_2$ in each organ was expressed as the percentage injected dose (%ID) per organ calculated as the total activity in the organ ROI (Bq)/injected dose (Bq) $\times$ 100.

The number of disintegrations per unit activity administered (residence time) was obtained using the ratio of the cumulative activity and injected dose for each subject. The cumulative activity was obtained from the area under the time-activity curve. The area under the curve was calculated as the trapezoid sum of the observed data and the integral of physical decay for the curve tail after the last scan. The remainder of the body, an important input parameter for OLINDA/EXM 1.1 software (Organ Level Internal Dose Assessment Code, Vanderbilt University, Nashville, TN), was also assessed. If excretion of the radiotracer is prevented, the total residence time, which is the summation of the residence times in all of the organs in the body and the remainder of the body, can be calculated using the following simple equation:

$$\text{Total residence time} = \frac{\int_0^\infty A_0 e^{-\lambda t} dt}{A_0} = \frac{1}{\lambda} = \frac{T_{1/2}}{\ln 2} \approx 1.443 \times T_{1/2},$$

where A_0 is the injected dose, λ is the decay constant, and $T_{1/2}$ is the physical half-life of the radioisotope. In this study, the total residence time was about 8.67 h because the half-life of ^{99m}Tc was 6.01 h. The excretion of the radiotracer was assessed by the total radiation counts inside of the body contour of the geometrically averaged whole-body images. The residence time in the remainder of the body was obtained from the total residence time, summation of residence times in all of the organs, and excretion from the body.

Finally, the calculated residence times in each organ and the remainder of the body were used as input parameters for the OLINDA/EXM 1.1 software. The OLINDA/EXM 1.1 reports individual organ doses for 24 organs, effective dose (ED), and effective dose equivalent (EDE) using residence time data with reference to adult male and female models. The EDE and ED were calculated as the weighted sum of each individual organ dose. The weighting factors for the EDE and ED were defined from International Commission of Radiation Protection (ICRP) publications 26 (1979) and 60 (1990).

Results

No adverse events were observed. Figure 2 shows a geometrically averaged whole-body image 0, 1, 2, 4, 8, and 24 h postinjection. After the intravenous injection, ^{99m}Tc-IDA-D-[c(RGDfK)]$_2$ was rapidly taken up by various tissues and organs. High accumulations were observed in the heart, liver, kidneys, and urinary bladder at the initial phase and in the large intestine only at a very late phase. The residence times and cumulative activity percentage in each organ are shown in Table 1; high residence times were reported in the liver, large intestine, urinary bladder, and kidneys. ^{99m}Tc-IDA-D-[c(RGDfK)]$_2$ was mainly eliminated through the hepatobiliary system and the renal system. Mean time-activity curves representing organ distribution details of %ID are shown in Figure 3. The radioactivity in the kidneys, liver, spleen, and brain decreased with time. Organs such as the urinary bladder, large intestine, and gallbladder showed initial accumulation and late washout according to the individuals' natural absorption and excretion cycles. At 24 h

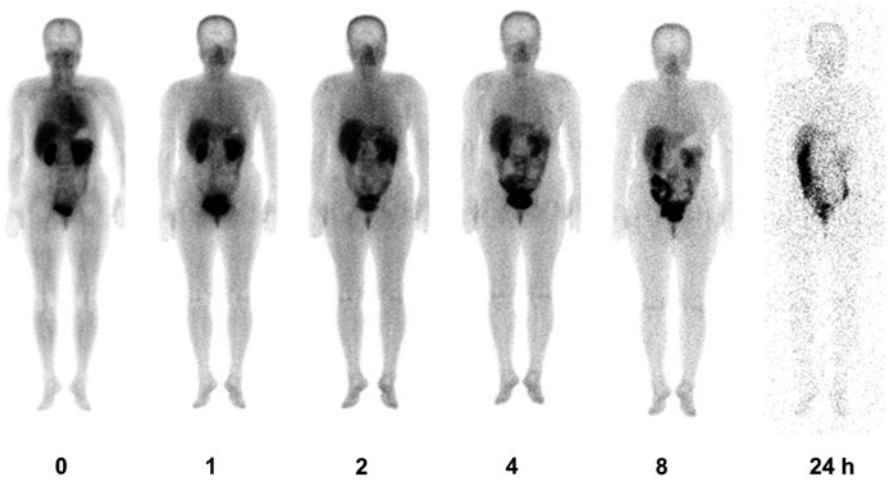

FIG. 2. Planar whole-body images showing biodistribution of ^{99m}Tc-IDA-D-[c(RGDfK)]$_2$ at different times after i.v. injection (from *left* to *right*, 0, 1, 2, 4, 8, and 24 h) in a healthy volunteer.

postinjection, the radioactivity of ^{99m}Tc-IDA-D-[c(RGDfK)]$_2$ in almost all of organs had diminished completely, except in the large intestine.

The radiation dose to each organ and the effective doses (ED and EDE) obtained using OLINDA/EXM software are listed in Table 2. As expected, high radiation doses were reported in the upper large intestine (19.28 ± 4.78 μGy/MBq), urinary bladder wall (19.15 ± 6.84 μGy/MBq), kidneys (15.67 ± 0.90 μGy/MBq), liver (9.13 ± 1.71 μGy/MBq), and gallbladder wall (9.09 ± 2.03 μGy/MBq). Whole-body mean EDE and ED were 7.11 ± 0.58 μGy/MBq and 5.08 ± 0.53 μGy/MBq, respectively.

Discussion

Recently, angiogenesis imaging targeting integrin $\alpha_v\beta_3$ has gained widespread attention due to its value in tumor diagnostics and therapy. Studies, including ours, assessing the correlation of angiogenic activity in tumors with overexpression of integrin $\alpha_v\beta_3$ and tumor metabolism using ^{99m}Tc-IDA-D-[c(RGDfK)]$_2$ SPECT and ^{18}F-fluorodeoxyglucose (^{18}F-FDG) PET, respectively, have reported on the clinical significance of angiogenesis imaging in solid tumor compared to metabolic imaging, compensating for the lack of biological characteristics in metabolic imaging.[13,16,21] Although ^{99m}Tc-IDA-D-[c(RGDfK)]$_2$ SPECT images demonstrated higher tumor-to-normal uptake ratios than ^{18}F-FDG PET images in glioma patients and have shown its clinical potential, readily available and cost-effective radiotracers for monitoring angiogenesis are yet to be developed.

Table 1. Cumulative Activity Percentages (%ID) and Mean Residence Times (h)

Organ	*%ID*	*Residence time (×100, h)*
Urinary Bladder	3.78 ± 2.08	0.33 ± 0.18
Brain	0.48 ± 0.24	0.04 ± 0.02
Gallbladder	0.25 ± 0.12	0.02 ± 0.01
Kidneys	2.97 ± 0.29	0.26 ± 0.03
Liver	6.09 ± 1.83	0.53 ± 0.16
Spleen	0.30 ± 0.23	0.03 ± 0.02
Large intestine	5.40 ± 1.51	0.47 ± 0.13
Total body	48.24 ± 3.86	5.85 ± 0.41
Remainder of the body	67.51 ± 4.70	4.18 ± 0.33
Outside of the body	32.49 ± 4.70	2.82 ± 0.41

Values are mean ± SD.

Radiotracers for angiogenesis imaging have a potentially broad field of application, spanning from cancer to cardiovascular theranostics. Several RGD peptides have been tested in the recent past, demonstrating that the number of RGD moieties, the isotope, and chelator profoundly affect the synthetic process, binding potential, and *in vivo* biodistribution.[22] Other research groups have tried to synthesize ^{99m}Tc-labeled RGD analogs containing various ^{99m}Tc-chelating moieties such as 2-mercaptoacetyl-glycylglycyl (MAG2) and 6-hydrazinonicotinamide (HYNIC).[23,24] However, these ^{99m}Tc-chelating moieties of the target compound have significant shortcomings, such as a bulky core size, low metabolic stability, and slow clearance from the normal tissue. Therefore, certain RGD analogs have been formulated to include polyethylene glycol (PEG4) or glycine (G3) linkers to increase the integrin $\alpha_v\beta_3$ binding affinity in a ''bivalent'' manner and to improve radiotracer excretion kinetics from normal organs.[24] IDA-D-[c(RGDfK)]$_2$ is a newly developed, cyclic synthetic ligand containing the RGD binding site with a high affinity for integrin $\alpha_v\beta_3$ during angiogenesis.[14]

SPECT/computed tomography (SPECT/CT) is a hybrid imaging modality that can longitudinally diagnose the target environment in the same subject across different time points noninvasively. RGD analogs that are labeled with radioisotopes suitable for SPECT detector systems, such as ^{99m}Tc, can be used as radiotracers for angiogenesis imaging with SPECT/CT. A clear advantage of the ^{99m}Tc-labeled SPECT radiotracer is its potential for clinical use as it is readily available and cost-effective compared to PET. ^{99m}Tc-labeled IDA-D-[c(RGDfK)]$_2$ is a newly developed radiotracer for SPECT (or gamma camera) to visualize angiogenic lesions and is a promising agent for cancer imaging.

Human internal radiation dosimetry for newly developed radiotracers is essential for the risk-benefit assessment of clinical applications, which might influence the choice of the radiotracer. Therefore, in the present study, the authors evaluated the radiation dose exposure in humans who underwent a whole-body ^{99m}Tc-IDA-D-[c(RGDfK)]$_2$ gamma camera scan. The results of the present study indicate that this tracer has

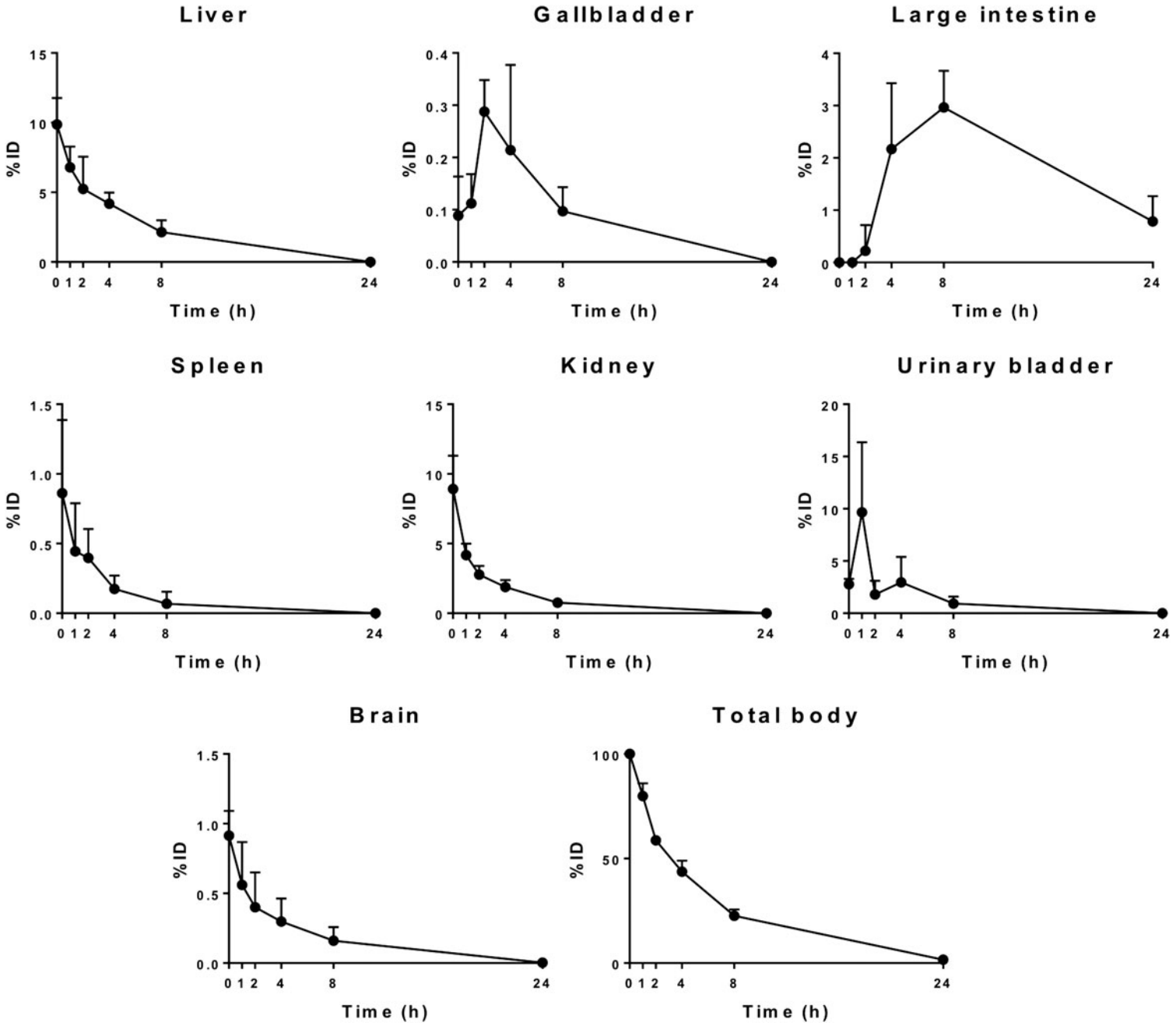

FIG. 3. Time-activity (%ID) curves for the organs. Data are mean ± SD.

Table 2. Organ Radiation Doses, Effective Doses, and Effective Dose Equivalents

Organ	*Radiation dose (μGy/MBq)*
Adrenals	4.81 ± 0.43
Brain	1.46 ± 0.33
Breasts	2.03 ± 0.26
Gallbladder wall	9.09 ± 2.03
Lower large intestine wall	4.44 ± 0.52
Small intestine	6.18 ± 0.78
Stomach wall	4.11 ± 0.48
Upper large intestine wall	19.28 ± 4.78
Heart wall	3.56 ± 0.40
Kidneys	15.67 ± 0.90
Liver	9.13 ± 1.71
Lungs	3.21 ± 0.42
Muscle	2.97 ± 0.29
Ovaries	5.56 ± 0.59
Pancreas	4.92 ± 0.49
Red marrow	3.07 ± 0.27
Osteogenic cells	7.77 ± 0.91
Skin	1.83 ± 0.19
Spleen	5.10 ± 1.72
Testes	2.72 ± 0.42
Thymus	2.80 ± 0.37
Thyroid	2.43 ± 0.21
Urinary bladder wall	19.15 ± 6.84
Uterus	5.70 ± 0.77
Effective dose equivalent (μSv/MBq)	7.11 ± 0.58
Effective Dose (μSv/MBq)	5.08 ± 0.53

Values are mean ± SD.

favorable whole-body pharmacokinetics in terms of its high renal and hepatic extraction, rapid clearance through the kidneys, gallbladder, and GI tract and low doses in the other organs. The kidney exhibited high accumulation, suggesting the possibility to be the dose-limiting organ when targeting integrin $\alpha_v\beta_3$ for antiangiogenic therapy. Although the high kidney accumulation is probably caused by the increased arginine residues, the kidney uptake is comparable to other radiolabeled multimeric cyclic RGD peptides and other peptides.[24–26] Activity in the liver and kidneys is substantially eliminated 8 h postinjection, with the excretion of the radiotracer through the large intestine and urinary bladder, with some residual activity in the large intestine. The ED and/or EDE values for other SPECT and/or gamma camera radiotracers commonly used clinically are listed in Table 3; the ED and EDE values for ^{99m}Tc-IDA-D-[c(RGDfK)]$_2$ are comparable to those of other ^{99m}Tc-labeled radiotracers. To their knowledge, their study is the first reported evaluation of the human internal dosimetry of ^{99m}Tc-IDA-D-[c(RGDfK)]$_2$ and represents an advancement in the quest for an ideal SPECT tracer for angiogenesis imaging.

The present study is limited by its small sample size. Because of the limited number of participants, the authors did not calculate the doses for subject-specific organ volumes. Rather, the authors computed the doses according to the OLINDA/EXM 1.1 reference phantoms. This approach is reasonable for low-dose range radiopharmaceutical compounds typically used in diagnostics, in which patient radioprotection is the main concern, because ED is a metric used for assessing stochastic risk in a population. On the contrary, the use of subject-specific organ masses would be crucial if a therapeutic approach was considered. Another limitation is the quantification of the dual-head gamma camera data. The geometric mean method using simultaneously acquired anterior and posterior images, which the authors adopted here, is certainly useful in activity quantification. However, its accuracy is limited to specific clinical situations. The most fundamental drawback of this method is the fact that it assumes constant attenuation of the photon intensity with the source depth; hence, it does not correct for the contribution of scatter to the counts obtained. This assumption is not valid for the relatively wide window settings used in nuclear medicine. It has been shown that the broad beam attenuation coefficient varies from 0.081 cm^{-1} for a source at 1-cm depth to 0.122 cm^{-1} for a source at 15-cm depth in tissue equivalent material using a 30% window. In addition, the method does not take into consideration the effects of the source thickness and inhomogeneity of the attenuating medium. The source thickness and inhomogeneity effects *in vivo* may be as high as 20% each.[31]

Table 3. The Effective Radiation Doses of ^{99M}Tc-Labeled Single Photon Emission Computed Tomography Radiotracers

Radiotracer	*Effective dose (μSv/MBq)*	*Effective dose equivalent (μSv/MBq)*	*Reference*
^{99m}Tc-IDA-D-[c(RGDfK)]$_2$	5.08	7.11	Herein
^{99m}Tc-MDP	5.70	N/A	27
^{99m}Tc-DTPA	N/A	8.91	28
^{99m}Tc-MAG3	N/A	10.00	28
^{99m}Tc-TRODAT-1	10.54	12.97	29
^{99m}Tc-MIBI	11.00	N/A	30

As mentioned earlier, integrin $\alpha_v\beta_3$ is a suitable target not only for tumor angiogenesis imaging but also for antiangiogenic therapy. In an aspect of radiotheranostics, the peptide IDA-D-[c(RGDfK)]$_2$ is possibly transformed into a therapeutic radiopharmaceutical compound when it is labeled with β-emitting radioisotopes such as rhenium-188 (^{188}Re), as previously reported.[14] Hence, target distribution and dosimetry studies of β-emitting radioisotope labeled IDA-D-[c(RGDfK)]$_2$ must be performed as previously mentioned, to utilize its strength as a radiotheranostic radiopharmaceutical. In specific, pretherapeutic scans with ^{99m}Tc-IDA-D[c[RGDfK]$_2$ could aid the decision process of ^{188}Re-IDA-D[c[RGDfK]$_2$ radiation dosage prescription, predicting the possible radiation accumulation to critical nontarget organs such as the kidney.

To conclude, the radiation dosimetry results for ^{99m}Tc-IDA-D-[c(RGDfK)]$_2$ are comparable to the data reported for other ^{99m}Tc-labeled radiotracers, and thus, possible diagnostic use of the new radiotracer does not escalate the radiation risk to the patient. This study demonstrates that ^{99m}Tc-IDA-D-[c(RGDfK)]$_2$ is an efficacious and safe radiotracer for imaging integrin $\alpha_v\beta_3$ expression.

Acknowledgments

The authors thank Bio Imaging Korea Co., Ltd. for providing the precursor for radiolabeling and helping with

radiolabeling procedures. This research was supported by the Korea Health Technology R&D Project through the Korea Health Industry Development Institute (KHIDI), funded by the Ministry of Health & Welfare, Republic of Korea (HI14C1072), and the Basic Science Research Program through the National Research Foundation of Korea (NRF), funded by the Ministry of Science and ICT, Republic of Korea (NRF-2013R1A1A2013175, NRF-2015R1D1A1A02061707, and NRF-2016R1D1A1A02937028).

Disclosure Statement

There are no existing financial conflicts.

References

1. Ferrara N. Role of vascular endothelial growth factor in regulation of physiological angiogenesis. Am J Physiol Cell Physiol 2001;280:C1358.
2. Neufeld G, Cohen T, Gengrinovitch S, et al. Vascular endothelial growth factor (VEGF) and its receptors. FASEB J 1999;13:9.
3. Veikkola T, Karkkainen M, Claesson-Welsh L, et al. Regulation of angiogenesis via vascular endothelial growth factor receptors. Cancer Res 2000;60:203.
4. Gaertner FC, Kessler H, Wester HJ, et al. Radiolabelled RGD peptides for imaging and therapy. Eur J Nucl Med Mol Imaging 2012;39 Suppl 1:S126.
5. Haubner R, Wester HJ. Radiolabeled tracers for imaging of tumor angiogenesis and evaluation of anti-angiogenic therapies. Curr Pharm Des 2004;10:1439.
6. Laverman P, Sosabowski JK, Boerman OC, et al. Radiolabelled peptides for oncological diagnosis. Eur J Nucl Med Mol Imaging 2012;39 Suppl 1:S78.
7. Brooks P, Clark R, Cheresh D. Requirement of vascular integrin alpha v beta 3 for angiogenesis. Science 1994; 264:569.
8. Ruoslahti E. Specialization of tumour vasculature. Nat Rev Cancer 2002;2:83.
9. Knetsch PA, Petrik M, Griessinger CM, et al. [^{68}Ga] NODAGA-RGD for imaging $\alpha_v\beta_3$ integrin expression. Eur J Nucl Med Mol Imaging 2011;38:1303.
10. Haubner R, Kuhnast B, Mang C, et al. [^{18}F]Galacto-RGD: Synthesis, radiolabeling, metabolic stability, and radiation dose estimates. Bioconjug Chem 2004;15:61.
11. Chen X, Park R, Tohme M, et al. MicroPET and autoradiographic imaging of breast cancer alpha v-integrin expression using ^{18}F- and ^{64}Cu-labeled RGD peptide. Bioconjug Chem 2004;15:41.
12. Mulder WJ, Griffioen AW. Imaging of angiogenesis. Angiogenesis 2010;13:71.
13. Beer AJ, Lorenzen S, Metz S, et al. Comparison of integrin alphaVbeta3 expression and glucose metabolism in primary and metastatic lesions in cancer patients: A PET study using ^{18}F-galacto-RGD and ^{18}F-FDG. J Nucl Med 2008;49:22.
14. Lee BC, Moon BS, Kim JS, et al. Synthesis and biological evaluation of RGD peptides with the ^{99m}Tc/^{188}Re chelated iminodiacetate core: Highly enhanced uptake and excretion kinetics of theranostics against tumor angiogenesis. RSC Adv 2013;3:782.
15. Yoo JS, Lee J, Jung JH, et al. SPECT/CT Imaging of High-Risk Atherosclerotic Plaques using Integrin-Binding RGD Dimer Peptides. Sci Rep 2015;5:11752.
16. Song YS, Park HS, Lee BC, et al. Imaging of Integrin alphavbeta3 Expression in Lung Cancers and Brain Tumors Using Single-Photon Emission Computed Tomography with a Novel Radiotracer (^{99m})Tc-IDA-D-[c(RGDfK)]2. Cancer Biother Radiopharm 2017;32:288.
17. Alberto R, Schibli R, Egli A, et al. A Novel Organometallic Aqua Complex of Technetium for the Labeling of Biomolecules: Synthesis of $[^{99m}Tc(OH_2)_3(CO)_3]^+$ from $[^{99m}TcO4]^-$ in Aqueous Solution and Its Reaction with a Bifunctional Ligand. J Am Chem Soc 1998;120:7987.
18. Chen B, Zhao G, Ma Q, et al. (^{99m})Tc-3P-RGD$_2$ SPECT to monitor early response to bevacizumab therapy in patients with advanced non-small cell lung cancer. Int J Clin Exp Pathol 2015;8:16064.
19. Jin X, Liang N, Wang M, et al. Integrin Imaging with ^{99m}Tc-3PRGD$_2$ SPECT/CT shows high specificity in the diagnosis of lymph node metastasis from non-small cell lung cancer. Radiology 2016;281:958.
20. Zhu Z, Miao W, Li Q, et al. ^{99m}Tc-3PRGD$_2$ for integrin receptor imaging of lung cancer: A multicenter study. J Nucl Med 2012;53:716.
21. Groves AM, Shastry M, Rodriguez-Justo M, et al. ^{18}F-FDG PET and biomarkers for tumour angiogenesis in early breast cancer. Eur J Nucl Med Mol Imaging 2011;38:46.
22. Liu S. Radiolabeled Cyclic RGD Peptide Bioconjugates as Radiotracers Targeting Multiple Integrins. Bioconjug Chem 2015;26:1413.
23. Decristoforo C, Santos I, Pietzsch HJ, et al. Comparison of in vitro and in vivo properties of [^{99m}Tc]cRGD peptides labeled using different novel Tc-cores. Q J Nucl Med Mol Imaging 2007;51:33.
24. Shi J, Kim YS, Zhai S, et al. Improving tumor uptake and pharmacokinetics of ^{64}Cu-labeled cyclic RGD peptide dimers with Gly(3) and PEG(4) linkers. Bioconjug Chem 2009;20:750.
25. Akizawa H, Arano Y, Mifune M, et al. Effect of molecular charges on renal uptake of ^{111}In-DTPA-conjugated peptides. Nucl Med Biol 2001;28:761.
26. Shi J, Kim YS, Chakraborty S, et al. 2-Mercaptoacetylglycyl glycyl (MAG2) as a bifunctional chelator for ^{99m}Tc-labeling of cyclic RGD dimers: Effect of technetium chelate on tumor uptake and pharmacokinetics. Bioconjug Chem 2009;20:1559.
27. Mhiri A, Slim I, Ghezaiel M, et al. Estimation of Radiation Dosimetry for some Common SPECT-CT Exams. International Journal of Biotechnology for Wellness Industries 2012;1:266.
28. Stabin M, Taylor A, Jr., Eshima D, et al. Radiation dosimetry for technetium-99m-MAG3, technetium-99m-DTPA, and iodine-131-OIH based on human biodistribution studies. J Nucl Med Jan 1992;33:33.
29. Mozley PD, Stubbs JB, Plossl K, et al. Biodistribution and dosimetry of TRODAT-1: a technetium-99m tropane for imaging dopamine transporters. J Nucl Med 1998;39: 2069.
30. Leide S, Diemer H, Ahlgren L, Mattsson S. In: Schlafke-Stelson AT (ed.), In vivo distribution and dosimetry of Tc-99m MIBI in man (CONF-910529–). United States 1992.
31. Hammond ND, Moldofsky PJ, Beardsley MR, et al. External imaging techniques for quantitation of distribution of I-131 F(ab')2 fragments of monoclonal antibody in humans. Med Phys 1984;11:778.